Thermophysical Properties of Nanoparticle-Enhanced Ionic Liquids (NEILs) Heat Transfer Fluids

Elise B. Fox, Ann E. Visser, Nicholas J. Bridges, and Jake W. Amoroso*

Savannah River National Laboratory, Aiken, SC 29808
*corresponding author: elise.fox@srnl.doe.gov, 803-507-8560

KEYWORDS: Nanoparticle Enhanced Ionic Liquid**,** 1-Butyl-2,3-dimethylimidazolium bis(trifluoromethylsulfonyl)imide, Thermal Conductivity, Heat Transfer Fluid

ABSTRACT

An experimental investigation was completed on nanoparticle enhanced ionic liquid heat transfer fluids as an alternative to conventional organic based heat transfer fluids (HTFs). These nanoparticle-based HTFs have the potential to deliver higher thermal conductivity than the base fluid without a significant increase in viscosity at elevated temperatures. The effect of nanoparticle morphology and chemistry on thermophysical properties was examined. Whisker shaped nanomaterials were found to have the largest thermal conductivity temperature dependence and were also less likely to agglomerate in the base fluid than spherical shaped nanomaterials.

INTRODUCTION

In many solar energy systems, such as concentrating solar power (CSP), there is a drive to operate at higher temperature to reach efficiency limits. This is often limited by the heat transfer fluids working window; it is desirable to have low temperature stability and expand the upper operating temperatures of the fluid. The current generation of organic heat transfer fluids, such as Therminol VP-1®, employ molecules that have significant vapor pressure within the temperature range for system operation.[1] The organic heat transfer fluids also decompose to produce hydrogen, which necessitates the use of palladium getters to absorb the hydrogen gas, which will cause embrittlement of the stainless steel receiver tube and can result in significant heat loss.[2] The HTFs may also form tars and sedimentation in system components and will cause increased wear, decrease the heat transfer properties, and increase costs due to increased system maintenance.

Recent efforts to expand the upper operating temperature for heat transfer fluids have focused on high temperature molten salts,[3-4] which can push the upper temperature limits for 900°C, but don't melt until 400°C.[5] This indicates either the need for heat tracing to prevent freezing in pipes or the search for alternatives that cannot operate at as high of temperatures, but have much lower freezing points. This has led to research in room-temperature molten salts, which are referred to as ionic liquids (IL). ILs have high heat capacities, a wide range of viscosities, and have been previously investigated as heat transfer and heat storage fluids.[6]

Nanofluids have also gained the attention of the heat transfer community for their promise of increased thermal conductivity of base fluids, though the results are often

conflicting.[7] Recently a round-robin study from thirty-four different institutions was conducted to help elucidate some of the conflicting evidence.[8] It was determined that thermal conductivity was enhanced with increasing particle loading and particle aspect ratio. It was also found that a majority of thermal conductivity measurements on the same solution were within 10%, regardless of the measurement technique used. Investigations of most recent nanofluids have focused on multi-walled carbon nanotubes,[9] and Al_2O_3[10] with a base solution of water or ethylene glycol.[11]

The intrinsically high heat capacity associated with nanoscale metals or metal oxides was used to enhance the properties of ILs to produce nanoparticle enhanced ionic liquids (NEILs) for use in solar energy applications has been previously demonstrated.[12] Here, the chemical and physical properties of a larger series of NEILs containing 1-butyl-2,3-methylimidazolium bis(trifluoromethylsulfonyl)imide were measured to determine how the presence of up to 10 weight percent nanoparticles affected the properties. These systems have increased our understanding of the effects of the addition of different kinds of nanoparticle to IL. Significant difference is observed between nanoparticles at very low loading.

EXPERIMENTAL

1-Butyl-2,3-dimethylimidazolium bis(trifluoromethylsulfonyl)imide [C_4mmim][Tf_2N] was used as received from Ionic Liquid Technologies, Inc. in an as received state. The water content of the ILs were measured by Karl Fisher titration and were nominally 200 ppm without additional drying. The nanoparticles were used as received from Aldrich Chemical Co., unless otherwise noted in Table 1. The nanoparticles were added to ILs by mass followed by vortex mixing (Fischer Scientific Heavy Duty Vortex Mixer 02-216-109) for fifteen minutes on medium-high speed (dial speed 8, approximately 1900rpm). The nanoparticles do not dissolve in the ILs, they typically form suspensions in the ILs. Experiments were typically run immediately after synthesis of the NEIL. If necessary, the nanomaterial would be re-suspended by vortexing for the proceeding experiment. Details on the suspensions and the suspendability limits are described within the results and discussion section. The physical properties of the nanomaterials are described in Table 1 below.

Characterization:

Thermogravimetric Analysis

All TGA experiments were conducted under a N_2 atmosphere using a Netzsch 209 F1 thermal gravimetric analyzer with single use Al crucibles at a ramp rate of 20°C/minute or 10°C/min. The thermal analysis software (Proteus V5.2.0) calculates the thermal onset temperature based on the intersection of the baseline with the tangent, at the inflection point, of the decomposition rate. Long term decomposition studies were conducted by heating the IL to a set temperature at a ramp rate of 20°C/min and holding for 120 minutes before progressing to the next set point with a ramp rate of 20°C/min.

Viscosity

Viscosity was measured using the cone and plate method on a Thermo Haake MARS III with Rheowin software. A 0.5° titanium cone and flat plate was used. All measurements were conducted at 25°C and duplicated. The instrument was calibrated with the appropriate NIST standard for the viscosity window of the material.

Thermal Conductivity

Thermal conductivity was measured using the transient hot wire method with a Decagon KD2 Thermal Properties Analyzer with the KS-1 sensor from 20-80°C. Samples were held at constant temperature in a heated water bath and allowed to equilibrate at temperature for 15 minutes before measurement. The bath was turned off during the measurements to avoid inducing convection in the IL. The uncertainty of the measurement is 5% or 0.01W/(m*K), per the manufacturer specifications.

Surface area

BET surface area was determined by a 17 point LN_2 absorption-desorption isotherm on a Micromeritics ASAP 2020C. The samples were degassed for a minimum of four hours at 120°C.

Particle Size Distribution

Particle size distribution was determined on a MicroTrac NanoTrack Ultra, which can detect particles from 1nm-7µm. Baseline measurements were obtained in the neat IL before testing the NEIL. The instrument was calibrated using NIST polystyrene sphere references suspended in the neat IL and in water.

Stereo Microscope Imaging

An Olympus SZX16 stereo microscope was used for low magnification imaging and an Olympus BX-41 laboratory microscope was used to obtain higher magnification images. Transmitted light was used for all imaging. Each sample was mixed for 10 minutes in a tumbler mixer and immediately afterwards, a single drop of each sample was placed onto a microscope slide for imaging.

RESULTS AND DISCUSSION

Thermal Stability

The $[C_4mmim][Tf_2N]$ IL was selected for these tests since ILs containing the imidazolium cations are commercially available, widely used, and have excellent thermal stability. The use of the C-2 methylation increases IL thermal stability[13] and decreases the interaction between the IL's cation and the nanoparticle, and the Tf_2N anion provides a thermally stable hydrophobic IL.[14] Other thermal stability studies of $[C_4mmim][Tf_2N]$ at a 10^oC/min heating rate show an onset temperature of approximately 485^oC[13] and a 5% mass loss temperature of 440^oC.[13] When the sample is heated at a faster heating rate, the decomposition temperatures increase due to the slow heat transfer in ILs. Thus, the temperature in the IL may lag behind.[15]

Using nanoparticles to affect the physical properties of ILs is a relatively recent application. In the literature, the addition of copper or graphite powder to long-chain $[C_nmim][Br]$ ILs causes only slight changes in the ILs melting and freezing temperatures.[16] Adding 0 – 25 wt% graphite powder to $[C_{16}mim][Br]$ affects the freezing temperature ±10°C. Kosmulski et al also show the addition of an unspecified amount of Al_2O_3 to $[C_8mim]_3PO_4$ has no impact on the thermal decomposition temperature.[17] Adding 10 wt% TiO_2, SiO_2, or Al_2O_3 to short-chain ILs affects the crystallinity of the plastic crystals.[18] The addition of nanoparticle powders to long-chain ILs also shows little effect on the thermodynamic properties of ILs.[19] Adding quartz or amorphous silica causes a significant increase in decomposition rate at 200°C

for $[C_6mim][PF_6]$ in air, but Al_2O_3 and TiO_2 have less of an effect, possibly due to the point of zero charge for each type of nanoparticles.[17]

The thermal stability was measured at 10°C/min for eleven NEILs and the results are shown in Table 2. The addition of 0.5 wt % nanoparticles to $[C_4mmim][Tf_2N]$ has essentially very little impact on the thermal stability when the experiments are performed at the relatively fast heating rate of at least 10 ^oC/min. The temperature for 5% weight loss was within a narrow temperature range of 9°C, from 421-430°C. The onset of decomposition had a much wider range of 29°C, from 444-473°C.

Increasing the nanoparticle loading up to 10 wt% has little effect on the measured temperature for 5% weight loss for both Al_2O_3 and carbon black as shown in Table 3. Larger differences can be seen when comparing the measured onset temperature. As Al_2O_3 is added up to 5 wt%, the onset temperature decreases 30°C before increasing with additional Al_2O_3 loading. The onset values for carbon black loaded $[C_4mmim][Tf_2N]$ vary by 10°C or less. This iterates the importance of closely examining experimental parameters in reported decomposition temperatures for ionic liquids.

To better assess the thermal stability of the ionic liquids and the effects of the nanomaterials on the NEIL stability, additional thermal testing was completed where samples were heated to temperature and the weight loss was measured at the elevated temperature over a two hour period. The mass loss for each NEIL per hour is reported in Table 4. These samples show a significant difference in the thermal stability. The Au containing NEIL behaved most similarly to the neat IL, which may be due to the large particle size of the Au, which was poorly stabilized in the IL. All other ILs were stable, without agitation, for the continuation of the 20 hour experiment, as observed by ex-situ samples.

When CuO, Fe_2O_3, SiO_2, and ZnO are used in the NEIL, all of the organic material is decomposed at 350°C. These four NEILs were made at a later date than the other NEILs. During the interim time, the bulk IL was stored under ambient conditions. It is possible that the storage of the IL allowed for a small amount of decomposition to occur. Small amounts of water could allow a reverse S_N2 reaction, yielding the primary alcohol and the neutral amine.[20-22] The effects of small amounts of impurities on the physical and chemical properties of NEILs will be addressed in a future publication.

When comparing NEILs with different particle morphology, but same elemental composition (whiskers vs. spheres), it is seen how the nanomaterial properties effect the overall thermal stability of the NEIL. The Al_2O_3 whiskers induce decomposition at lower temperatures than the spheres, which may be due to increased turbulence along the whisker.[23] When comparing carbon containing samples in Table 4, it is seen that not only does physical morphology affect the NEIL properties, but so does carbon hybridization. The amorphous carbon black, which was highly dispersed and created a more viscous fluid, had lower decomposition rates at 350°C than the three graphitized carbons, multi-walled carbon nanotube (MWCNT), single wall carbon nanotubes (SWCNT), and stacked graphene nanofiber (SGNF). Differences were also found among these three carbons, with faster decomposition occurring with SGNF > SWCNT > MWCNT.

Particle Size Distribution and Dispersability

In order to determine if there is particle agglomeration in the NEIL, particle size analysis was completed on NEILs with the base fluid $[C_4mmim][Tf_2N]$ and the various nanomaterials studied throughout the course of this project. Details on the physical properties of the

nanomaterials, such as dimension and surface area are reported in Table 1. The dimensions listed were those reported directly by the manufacturer, except for the Ketjen carbon black, which was determined from the BET analysis.

In the spherical shaped particles, the only particle that did not exhibit any agglomeration was the gold, which had a size distribution between 1-10nm. Interestingly, this particle formed the least stable suspension, which may be partially accounted for by the low surface area of the nanomaterial. The next smallest particle distribution was SiO_2 from 145-172 nm. Based on a manufacturer reported particle size of 5-15nm, the agglomerates could contain between 10-34 particles each. The next largest agglomeration occurs in ZnO, which had two distinct regions, 51% of the material was in the 102-486nm region and the remaining 49% was in the 1.3-2.8μm region. All other spherical shaped particles formed agglomerates that were larger than 2.3μm. The smallest nanomaterial, carbon black, formed the largest agglomerates, which were all larger than 5.5μm. The particle size distribution of all particles can be found in Figure 1.

The tubular or fiber-like nanomaterials had less of a tendency to agglomerate, as seen in Figure 2. The SGNF, measured between 1.2-1.6μm in diameter, which is within range of the reported lengthwise dimension of 1-10μm. The SWCNT measured distribution was between 0.09-0.24μm. This is slightly lower than the manufactures reported length of 0.5-10μm, which suggests that the SWCNT may break up upon agitation. The MWCNT had a measured distribution of 2.7-6.5μm, which is comparable to the manufacture's reported length of 1-5μm. The Al_2O_3 whiskers had two separate areas of particle sizes. Nominally, 19% of the particles were measure in length of 0.49-1.2μm. This is less than the manufacture's reported length of 2.8μm, which suggests that at least some of the whiskers break-up during agitation and are freely dispersed. The remaining 81% of the whiskers are reported from 3.3-6.6μm, indicating that there is small agglomeration of the whiskers.

The nanomaterial used would affect how long the NEIL remained dispersed. For example, with Au nanomaterial (NM) would nearly immediately fall out of suspension and would only remain suspended for the length of time needed to complete a single thermal conductivity measurement or particle size distribution measurement (approximately two minutes). Other NMs, such as CB and SiO_2, remained completely dispersed for over a month without additional agitation, the longest period of time observed. In order to better investigate the dispersity, stereomicroscope images were taken of droplets of the Al_2O_3 spheres and whiskers, carbon black, and MWCNT NEILs. The drop sizes ranged from 5-8mm, as seen in the inset images in Figure 3. All of the NM agglomerated in some manner. The Al_2O_3 spheres were loosely organized in clusters 100μm or larger, with smaller, more concentrated clusters dispersed within. The Al_2O_3 whiskers were more tightly bound in smaller clusters 25μm or smaller in size. Carbon black had the highest dispersion, forming a loosely interconnected network of chains and clumps 40μm or less, while the MWCNT formed clusters approximately 20μm in diameter and exhibiting similar behavior to the Al_2O_3 whiskers.

Viscosity

The Tf_2N^- anion was selected for this study since ILs with that anion has both relatively low viscosity and increased thermal stability. The viscosity for neat [C_4mmim][Tf_2N] has been reported several times and the data are consistent; 105cP at 21°C,[24] 97.1cP at 25°C,[25] and approximately 100cP at 25°C.[26] Here, the neat [C_4mmim][Tf_2N] viscosity is 99.6cP at 25°C and closely agrees with the reported values in previous literature. Figure 4 shows the viscosity at 25°C of [C_4mmim][Tf_2N] containing 0.5 wt% nanoparticles.

The presence of 0.5 wt% SiO_2, Al_2O_3, Au, ZnO, CuO, Fe_2O_3, or SGNF in this IL yields viscosity in the range of 101 – 105cP, as seen in Figure 3. With 0.5 wt% MWCNT, the viscosity increases to 110cP. Adding 0.5 wt% carbon black increases the viscosity to 150cP, due to the high pore volume and surface area of the nanoparticle. Carbon black fillers have been shown at loadings has low as 10% to have such a large influence on viscosity to induce gel behavior[27] and decrease elastic memory[28] in melts. Higher concentrations of Al_2O_3 nanoparticles further increase the viscosity, as seen in Figure 5.[12] Few other reports include viscosity measurements of ILs containing small amounts of nanoparticles.[29-30] IL-functionalized multi walled carbon nanotubes have been prepared and added to a neat IL and the viscosity of the resulting nanofluid was lower than the neat IL due to the lubricating properties of carbon nanotubes.[31]

The effect of various weight loadings of Al_2O_3 spheres on the viscosity of the NEIL at elevated temperatures was measured and is reported in Figure 5. At all temperatures, there is little measured difference in the viscosity of the neat IL and NEIL with 0.5 wt% Al_2O_3 spheres. When 2.5 wt% is added, there is 40cP increase in viscosity. As the temperature slowly increases, the difference in viscosity quickly drops to 30cP at 40°C, 20cP at 60°C, 15cP at 80°C, 10cP at 100°C and only 0.5cP difference at 300°C.

Thermal Conductivity

Thermal conductivity data at 50°C at ambient pressure for the IL and associated NEILs are shown in Figure 6. The thermal conductivity of neat $[C_4mmim][Tf_2]$ is nominally $0.13 Wm^{-1}K^{-1}$ almost independent of temperature over the range investigated which is similar to the behavior of many other ILs.[32-33] The low thermal conductivity result indicates this IL is a relatively poor thermal conductor since its thermal conductivity is approximately 22% lower than that of water. However, the thermal conductivity for Therminol VP-1 is 0.135 to $0.132 Wm^{-1}K^{-1}$ at 30 to 60°C, respectively, which is almost the same as that for IL and the NEILs.[1] In this case, only three nanomaterials were shown to increase the thermal conductivity of the IL: Al_2O_3 spheres, Al_2O_3 whiskers, and MWCNT. The data show most nanoparticles had little effect on the thermal conductivity of $[C_4mmim][Tf_2N]$. Addition of 0.5 wt% alumina spheres, whiskers, or MWCNT show an enhancement on the thermal conductivity of up to 3%, 6%, or 4%, respectively at 50°C. However, adding alumina whiskers yielded a thermal conductivity increase of 6% while alumina spheres was half of that, indicating the shape of the nanoparticle is important. This is in accordance with Buongiorno et al.[8], who found that with increasing particle aspect ratio, there was an increasing effect on thermal conductivity. There are multiple mechanisms proposed to explain the thermal conductivity enhancement of nanofluids.[34-35] Depending on the IL, the addition of MWCNT has previously produced both temperature dependent and temperature independent thermal conductivity enhancements, with no clear correlation between IL cation and anion identity.[36] All other nanoparticles tested here caused either no improvement or a decrease in the thermal conductivity in comparison to the neat IL.

The trends for thermal conductivity from room temperature to 60°C for the neat IL and the NEIL with the Al_2O_3 spheres and whiskers are plotted in Figure 7. For the neat IL, increasing temperature had very little effect on the thermal conductivity. The only other previously reported values for the thermal conductivity of $[C_4mmim][Tf_2N]$ are reported in[37], where the computational predictions (0.9-1.3W/(m*K)) were approximately 20% below experimental values. It can also be seen that the shape of the nanomaterial has a large effect on the thermal conductivity with temperature. There is an increase in thermal conductivity for both NEILs with both nanomaterials, but the effect is much more dramatic for the

whisker-shaped NEIL.

The thermal conductivity for the NEILs with carbonaceous materials from room temperature to 60°C is compared in Figure 8. Like the neat IL, the thermal conductivity for the carbon black and SGNF NEILs are relatively unchanged over the temperature range measured. The MWCNT NEIL initially has a thermal conductivity 4% higher than the neat IL. This rapidly decreases to that of the neat IL so that no benefit from the addition of the nanoparticle is observed. The SWCNT NEIL also sees a slight decline in thermal conductivity over the temperature range observed.

Understanding thermal conductivity enhancement in traditional nanofluids has been discussed in numerous papers. Maxwell's model for the dispersion of millimeter and micrometer-sized particles in a fluid shows the ratio between the thermal conductivity of the mixture and that of the base fluid depends on the thermal conductivity of both the solid and the liquid and on the volume fraction of the solid.[36] Expanding the model to account for the shape of the particles (e.g., other than spheres) and interactions between particles does not provide an accurate prediction of the thermal conductivity enhancement. Various mechanisms have been proposed to account for the phenomena; Brownian motion of the nanoparticles, liquid stacking at the particle/liquid interface, inherent means of heat transport within the nanoparticles, nanoparticle clustering[38] and particle surface chemistry.[8, 36]

The mechanism for enhanced thermal conductivity in NEILs is not clear. Molecular dynamics simulations for solvation of a 2nm ruthenium particle in ILs reveals the nanoparticles are solvated preferentially by the charged species of the IL ions and both the cation and anion are in contact with the nanoparticle.[39] A mixture of 10-20nm silica in 1-butyl-3-methylimidazolium Tf_2N showed no drastic changes in the C-H bands in the presence of nanosilica at ambient pressure, suggesting the lack of interaction between the silica and the IL ions.[40] X-ray photoelectron spectroscopy suggests the IL cation interacts very strongly with the surface of the carbon black and carbon black surface area decreases by 30%.[41] In comparison, Raman analysis of carbon nanotubes in 1-butyl-3-methylimidazolium hexafluorophosphate show the interactions between the IL and the nanotube are very weak.[42]

In these experiments, the majority of NEILs have thermal conductivities lower than that of the neat IL. Several ceramic oxides, metal, and carbon based materials were tested and only alumina and MWCNT produced an increased thermal conductivity, showing the complexity underlying the selection of nanoparticle to produce nanofluids with the desired properties.

CONCLUSIONS

This study demonstrates that the addition of inorganic nanoparticles can improve the thermal conductivity of an IL, dependant upon the selection of the nanomaterial. Nanoparticle Enhanced Ionic Liquids (NEILs) were prepared in $[C_4mmim][Tf_2N]$ and show the thermal stability is not compromised upon the addition of up to 10 wt% nanoparticles, regardless of the nanomaterial used. However, the diagreement in decomposition temperatures reported at a 10°C/min ramp rate and at a 5% wt loss of each NEIL suggest that careful consideration to experiemntal parameters must be considered when comparing expiermental data and attemptingt o determine a "true" decomposition temperature for ionic liquids. The viscosity of the NEILs is highly dependent on the type of nanoparticle added and is also likely influenced by the surface area of the nanoparticle. Viscocity is also highly temperature dependent and rapidly decreases with increasing temperature.

The thermal conductivity of the NEIL is typically independent of temperature (neat

IL, CB, SGNF), but in other cases, the morphology and chemistry of the nanoparticle appears to play a role in the conducticity. The presence of tube or whisker like structures induce temperature dependent changes in the thermal conductivity. In the case of MWCNT and SWCNT, a decrease in thermal conductivity with increasing temperature is observed, while with Al_2O_3 whiskers, an increase in thermal conductivity with increasing temperature is observed. All of these observed properties iterate the inherient compexity of designing nanofluids. Careful attention must be paid to the nanomaterial chemistry and morphology, while preventing adverse effects from occuring on the base fluid, such as an increase in decomposition or increase in viscocity.

ACKNOWLEDGEMENTS

Funding for this work is greatfully acknowledged from the DOE-EERE Solar Energy Techology Program. Savannah River National Laboratory is operated by Savannah River Nuclear Solutions. This document was prepared in conjunction with work accomplished under Contract No. DEAC09-08SR22470 with the U.S. Department of Energy.

REFERENCES

1. *Therminol vp-1 technical bulletin 7239115c*; Solutia: St. Louis, MO, 2008.
2. Moens, L. B., D. M.; In *Mechanism of hydrogen formation in solar parabolic trough receivers (sol-08-1108)*, 2008; 2008.
3. Nunes, V. M. B.; Lourenço, M. J. V.; Santos, F. J. V.; Nieto de Castro, C. A., Importance of accurate data on viscosity and thermal conductivity in molten salts applications†. *Journal of Chemical & Engineering Data* 2003, *48* (3), 446-450.
4. Burkhardt, J. J.; Heath, G. A.; Turchi, C. S., Life cycle assessment of a parabolic trough concentrating solar power plant and the impacts of key design alternatives. *Environmental Science & Technology* 2011, *45* (6), 2457-2464.
5. Williams, D. F., Assessment of candidate molten salt collants for the ngnp/nhi heat-transfer loop. *US DOE Report ORNL/TM-2006/69* 2006.
6. Wu, B. R., R. G.; Rogers, R. D. In *Novel ionic liquid thermal storage for solar thermal electric power systems*, 2001; 2001.
7. Nie, C.; Marlow, W. H.; Hassan, Y. A., Discussion of proposed mechanisms of thermal conductivity enhancement in nanofluids. *Int. J. Heat Mass Transfer* 2008, *50*, 1342-1348.
8. Buongiorno, J.; Venerus, D. C.; Prabhat, N.; McKrell, T.; Townsend, J.; Christianson, R.; Tolmachev, Y. V.; Keblinski, P.; Hu, L.-w.; Alvarado, J. L.; Bang, I. C.; Bishnoi, S. W.; Bonetti, M.; Botz, F.; Cecere, A.; Chang, Y.; Chen, G.; Chen, H.; Chung, S. J.; Chyu, M. K.; Das, S. K.; Paola, R. D.; Ding, Y.; Dubois, F.; Dzido, G.; Eapen, J.; Escher, W.; Funfschilling, D.; Galand, Q.; Gao, J.; Gharagozloo, P. E.; Goodson, K. E.; Gutierrez, J. G.; Hong, H.; Horton, M.; Hwang, K. S.; Iorio, C. S.; Jang, S. P.; Jarzebski, A. B.; Jiang, Y.; Jin, L.; Kabelac, S.; Kamath, A.; Kedzierski, M. A.; Kieng, L. G.; Kim, C.; Kim, J.-H.; Kim, S.; Lee, S. H.; Leong, K. C.; Manna, I.; Michel, B.; Ni, R.; Patel, H. E.; Philip, J.; Poulikakos, D.; Reynaud, C.; Savino, R.; Singh, P. K.; Song, P.; Sundararajan, T.; Timofeeva, E.; Tritcak, T.; Turanov, A. N.; Vaerenbergh, S. V.; Wen, D.; Witharana, S.; Yang, C.; Yeh, W.-H.; Zhao, X.-Z.; Zhou, S.-Q., A benchmark study on the thermal conductivity of nanofluids. *Journal of Applied Physics* 2009, *106* (9), 094312.
9. Garg, P.; Alvarado, J. L.; Marsh, C.; Carlson, T. A.; Kessler, D. A.; Annamalai, K., An experimental study on the effect of ultrasonication on viscosity and heat transfer performance of multi-wall carbon nanotube-based aqueous nanofluids. *International Journal of Heat and Mass Transfer* 2009, *52* (21–22), 5090-5101.
10. Timofeeva, E. V.; Gavrilov, A. N.; McCloskey, J. M.; Tolmachev, Y. V.; Sprunt, S.; Lopatina, L. M.; Selinger, J. V., Thermal conductivity and particle agglomeration in alumina nanofluids: Experiment and theory. *Physical Review E* 2007, *76* (6), 061203.
11. Wang, X.-Q.; Mujumdar, A. S., Heat transfer characteristics of nanofluids: A review. *International Journal of Thermal Sciences* 2007, *46* (1), 1-19.
12. Bridges, N. J.; Visser, A. E.; Fox, E. B., Potential of nanoparticle-enhanced ionic liquids (neils) as advanced heat-transfer fluids. *Energy Fuels* 2011, *25* (10), 4862-4864.
13. Fox, D. M.; Awad, W. H.; Gilman, J. W.; Maupin, P. H.; De Long, H. C.; Trulove, P. C., Flammability, thermal stability, and phase change characteristics of several trialkylimidazolium salts. *Green Chemistry* 2003, *5* (6), 724-727.
14. Fredlake, C. P.; Crosthwaite, J. M.; Hert, D. G.; Aki, S.; Brennecke, J. F., Thermophysical properties of imidazolium-based ionic liquids. *Journal of Chemical and Engineering Data* 2004, *49* (4), 954-964.
15. Kosmulski, M.; Gustafsson, J.; Rosenholm, J. B., Thermal stability of low temperature ionic liquids revisited. *Thermochimica Acta* 2004, *412* (1–2), 47-53.
16. Bai, L. G.; Li, X. M.; Zhu, J. Q.; Chen, B. A. H., Effects of nucleators on the thermodynamic properties of seasonal energy storage materials based on ionic liquids. *Energy & Fuels* 2011, *25* (4), 1811-1816.
17. Kosmulski, M.; Gustafsson, J.; Rosenholm, J. B., Thermal stability of low temperature ionic liquids revisited. *Thermochimica Acta* 2004, *412* (1-2), 47-53.
18. Pringle, J. M.; Shekibi, Y.; MacFarlane, D. R.; Forsyth, M., The influence of different nanoparticles on a range of organic ionic plastic crystals. *Electrochimica Acta* 2010, *55* (28), 8847-8854.
19. Hong, S. Y.; Im, J.; Palgunadi, J.; Lee, S. D.; Lee, J. S.; Kim, H. S.; Cheong, M.; Jung, K. D., Ether-functionalized ionic liquids as highly efficient so(2) absorbents. *Energy & Environmental Science* 2011, *4* (5), 1802-1806.
20. Wooster, T. J.; Johanson, K. M.; Fraser, K. J.; MacFarlane, D. R.; Scott, J. L., Thermal degradation of cyano containing ionic liquids. *Green Chem.* 2006, *8*, 671-6.
21. Gordon, J. E., Fused organic salts. Iii- chemical stability of molten tetra-n-alkylammonium salts. Medium effects on thermal r4n+x decomposition. Rbr + i^- = $ribr^-$ equilibrium constant in fused salt medium. *J. Org. Chem.* 1965, *30* (8), 2760-2763.
22. Scammells, P. J.; Scott, J. L.; Singer, R. D., Ionic liquids: The neglected issues. *Aust. J. Chem.* 2005, *58*, 155-169.
23. Kakaç, S.; Pramuanjaroenkij, A., Review of convective heat transfer enhancement with nanofluids. *International Journal of Heat and Mass Transfer* 2009, *52* (13–14), 3187-3196.
24. Andre, F.; Hapiot, P.; Lagrost, C., Dimerization of ion radicals in ionic liquids. An example of favourable "coulombic" solvation. *Physical Chemistry Chemical Physics* 2010, *12* (27), 7506-7512.
25. McLean, A. J.; Muldoon, M. J.; Gordon, C. M.; Dunkin, I. R., Bimolecular rate constants for diffusion in ionic liquids. *Chemical Communications* 2002, (17), 1880-1881.

26. Yan, C.; Zaijun, L.; Hailang, Z.; Yinjun, F.; Xu, F.; Junkang, L., 1-alkyl-2,3-dimethylimidazolium bis(trifluoromethanesulfonyl)imide ionic liquids as highly safe electrolyte for li/lifepo4 battery. *Electrochimica Acta* 2010, *55* (16), 4728-4733.

27. Lobe, V. M.; White, J. L., An experimental study of the influence of carbon black on the rheological properties of a polystyrene melt. *Polymer Engineering & Science* 1979, *19* (9), 617-624.

28. White, J. L.; Crowder, J. W., The influence of carbon black on the extrusion characteristics and rheological properties of elastomers: Polybutadiene and butadiene–styrene copolymer. *Journal of Applied Polymer Science* 1974, *18* (4), 1013-1038.

29. Ueno, K.; Imaizumi, S.; Hata, K.; Watanabe, M., Colloidal interaction in ionic liquids: Effects of ionic structures and surface chemistry on rheology of silica colloidal dispersions. *Langmuir* 2008, *25* (2), 825-831.

30. Wang, B.; Wang, X.; Lou, W.; Hao, J., Ionic liquid-based stable nanofluids containing gold nanoparticles. *J Colloid Interface Sci* 2011, *362* (Copyright (C) 2011 U.S. National Library of Medicine.), 5-14.

31. Wang, B.; Wang, X.; Lou, W.; Hao, J., Rheological and tribological properties of ionic liquid-based nanofluids containing functionalized multi-walled carbon nanotubes. *J. Phys. Chem. C* 2010, *114* (Copyright (C) 2011 American Chemical Society (ACS). All Rights Reserved.), 8749-8754.

32. Van Valkenburg, M. E.; Vaughn, R. L.; Williams, M.; Wilkes, J. S., Thermochemistry of ionic liquid heat-transfer fluids. *Thermochim. Acta* 2005, *425* (1-2), 181-188.

33. Chen, H.; He, Y.; Zhu, J.; Alias, H.; Ding, Y.; Nancarrow, P.; Hardacre, C.; Rooney, D.; Tan, C., Rheological and heat transfer behaviour of the ionic liquid, c(4)mim ntf2. *Int. J. Heat Fluid Flow* 2008, *29* (1), 149-155.

34. Wang, B. G.; Wang, X. B.; Lou, W. J.; Hao, J. C., Ionic liquid-based stable nanofluids containing gold nanoparticles. *Journal of Colloid and Interface Science* 2011, *362* (1), 5-14.

35. Keblinski, P.; Phillpot, S. R.; Choi, S. U. S.; Eastman, J. A., Mechanisms of heat flow in suspensions of nano-sized particles (nanofluids). *Int. J. Heat Mass Transf.* 2002, *45* (4), 855-863.

36. Nieto de Castro, C. A.; Lourenço, M. J. V.; Ribeiro, A. P. C.; Langa, E.; Vieira, S. I. C.; Goodrich, P.; Hardacre, C., Thermal properties of ionic liquids and ionanofluids of imidazolium and pyrrolidinium liquids†. *Journal of Chemical & Engineering Data* 2009, *55* (2), 653-661.

37. Liu, H.; Maginn, E.; Visser, A. E.; Bridges, N. J.; Fox, E. B., Thermal and transport properties of six ionic liquids: An experimental and molecular dynamics study. *Industrial & Engineering Chemistry Research* 2012, *51* (21), 7242-7254.

38. Prasher, R.; Phelan, P. E.; Bhattacharya, P., Effect of aggregation kinetics on the thermal conductivity of nanoscale colloidal solutions (nanofluid). *Nano Letters* 2006, *6* (7), 1529-1534.

39. Pensado, A. S.; Pádua, A. A. H., Solvation and stabilization of metallic nanoparticles in ionic liquids. *Angew. Chem. Int. Ed.* 2011, *50* (37), 8683-8687.

40. Chang, H.-C.; Hung, T.-C.; Chang, S.-C.; Jiang, J.-C.; Lin, S. H., Interactions of silica nanoparticles and ionic liquids probed by high pressure vibrational spectroscopy. *The Journal of Physical Chemistry C* 2011, *115* (24), 11962-11967.

41. Lei, Y.; Guo, B.; Liu, X.; Jia, D., Structure evolution of carbon black under ionic-liquid-assisted microwave irradiation. *Applied Surface Science* 2009, *255* (20), 8488-8493.

42. Wang, J.; Chu, H.; Li, Y., Why single-walled carbon nanotubes can be dispersed in imidazolium-based ionic liquids. *ACS Nano* 2008, *2* (12), 2540-2546.

Table 1. Physical properties of nanomaterials used in this study.

Nanomaterial	Dimension(s)/ nm [#]	Surface area/ m^2	Pore volume/ cm^3/g
Al_2O_3 spheres	<50nm	142	0.79
Al_2O_3 whiskers	2-4nm x 2800nm	283	0.21
Carbon black (Ketjen)	4 [&]	1410	2.72
MWCNT (Strem)	20-25nm x 1-5μm	194	0.65
SWCNT (Bucky USA)	0.7-2.5nm x 0.5-10μm	1115	0.98
SGNF (Strem)	40-50nm x 1-10μm	164	0.40
ZnO	<50nm	25	0.07
Fe_2O_3	<50nm	32	0.08
SiO_2	5-15	512	0.52
CuO	<50nm	16	0.04
Au	<100nm	2	$5.01x10^{-3}$

= dimensions as reported by manufacturer, unless otherwise noted

[&] = dimension as determined by BET

Table 2. Thermal Decomposition Temperatures for [C_4mmim][Tf_2N] containing various nanoparticles at a 10 ^{o}C/min heating rate.

Wt % Nanoparticle	Temperature for 5% Wt Loss/ °C	Onset/ ^{o}C
Neat IL	430	459
0.5% SiO_2	425	449
0.5% Al_2O_3 whiskers	427	473
0.5% Al_2O_3 spheres	420	446
0.5% Au	425	456
0.5% ZnO	429	451
0.5% CuO	425	449
0.5% Fe_2O_3	421	445
0.5% SGNF	428	450
0.5% MWCNT	427	452
0.5% SWCNT	425	444
0.5% Carbon Black	424	448

Table 3. Thermal Decomposition of $[C_4mmim][Tf_2N]$ With Increased NP Loading (10 ^oC/min heating rate)

Wt % Nanoparticle	**Onset/ ^oC**	**Temperature for 5% Wt Loss/ °C**
0.5% Al_2O_3 sphere	446	420
2.5% Al_2O_3 sphere	429	421
5% Al_2O_3 sphere	416	416
7.5% Al_2O_3 sphere	444	419
10% Al_2O_3 sphere	437	417
0.5% Carbon Black	448	424
1% Carbon Black	447	410
2.5% Carbon Black	455	424
5% Carbon Black	444	415
7.5% Carbon Black	454	423
10% Carbon Black	444	414

Table 4. Static decomposition rates of the IL as a function of temperature in 0.5% NEIL.

	% Mass Loss per Hour at Temperature								
Sample	**200°C**	**225°C**	**250°C**	**275°C**	**300°C**	**325°C**	**350°C**	**375°C**	**400°C**
$[C_4mmim][Tf_2N]$	0.00	0.04	0.06	0.16	0.37	1.42	4.07	10.31	17.60
$[C_4mmim][Tf_2N]$ + $Al_2O_{3\ sphere}$	0.00	0.00	0.00	0.26	0.90	2.48	5.23	11.83	20.21
$[C_4mmim][Tf_2N]$ +$Al_2O_{3\ whiskers}$	0.00	0.00	0.03	0.35	1.74	5.97	14.88	19.00	5.32
$[C_4mmim][Tf_2N]$ + CB	0.11	0.07	0.18	0.39	0.95	1.97	5.20	19.37	22.92
$[C_4mmim][Tf_2N]$ + SGNF	0.00	0.03	0.15	0.60	2.18	5.72	23.07	19.72	5.95
$[C_4mmim][Tf_2N]$ + MWCNT	0.00	0.00	0.02	0.19	1.02	4.37	11.06	18.37	7.18
$[C_4mmim][Tf_2N]$ + SWCNT	0.00	0.00	0.02	0.27	1.23	6.85	17.01	21.47	0.32
$[C_4mmim][Tf_2N]$ + Au	0.00	0.00	0.10	0.35	0.74	1.87	4.95	11.50	18.24
$[C_4mmim][Tf_2N]$ + CuO	0.05	0.08	0.28	1.06	6.19	13.21	22.68	N/A	N/A
$[C_4mmim][Tf_2N]$ + Fe_2O_3	0.06	0.12	0.38	1.44	4.86	11.82	22.55	N/A	N/A
$[C_4mmim][Tf_2N]$ + SiO_2	0.03	0.06	0.21	1.14	3.28	7.22	18.89	N/A	N/A
$[C_4mmim][Tf_2N]$ + ZnO	0.03	0.06	0.19	0.72	2.74	6.71	16.77	N/A	N/A

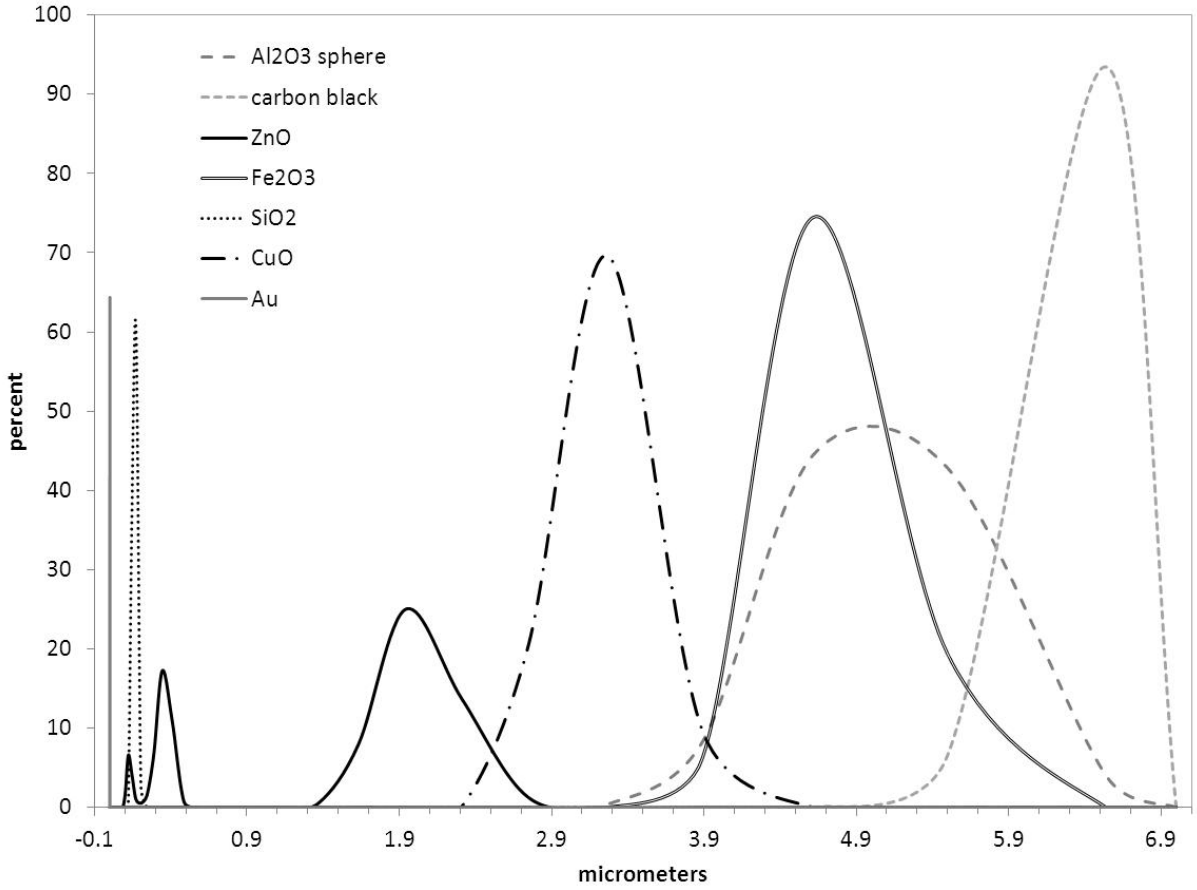

Figure 1. Particle size distribution of spherical shaped nanomaterials in [C_4mmim][Tf_2N].

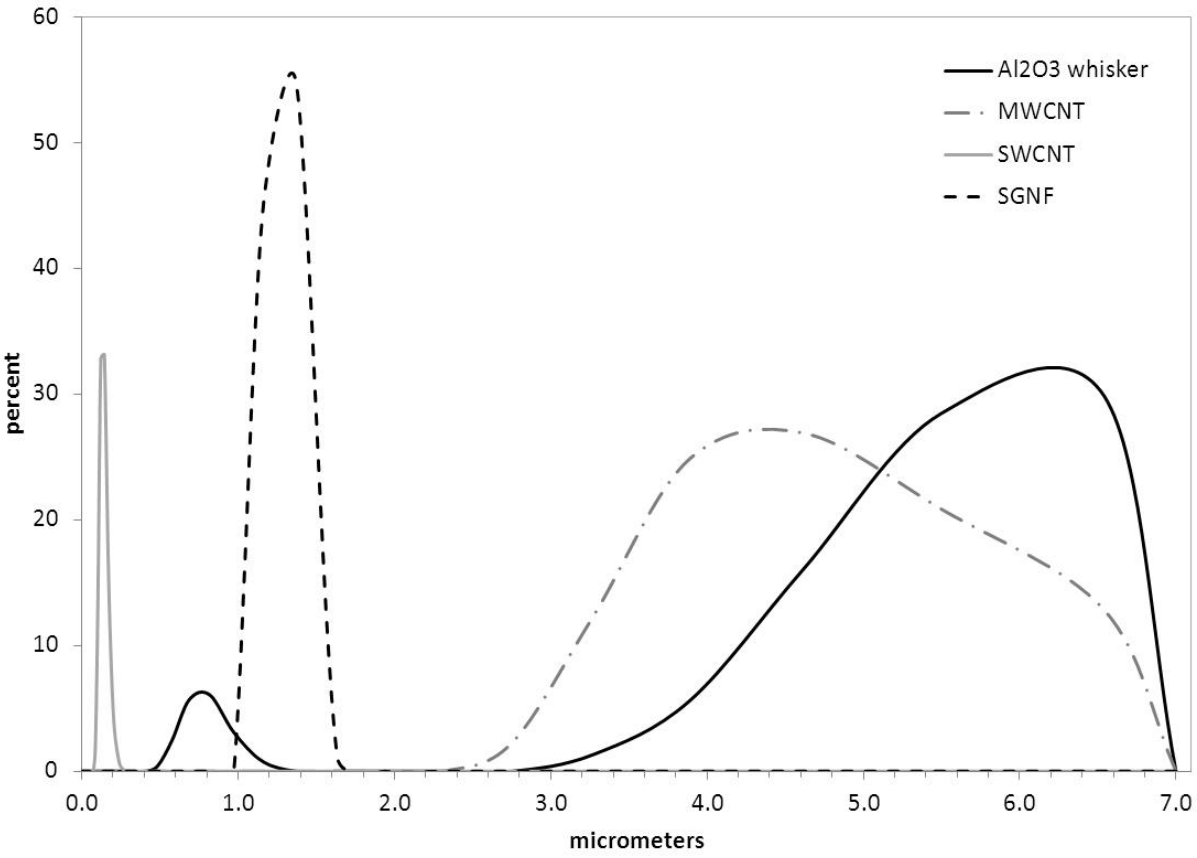

Figure 2. Particle size distribution of tubular or fiber-like nanomaterials in [C_4mmim][Tf_2N].

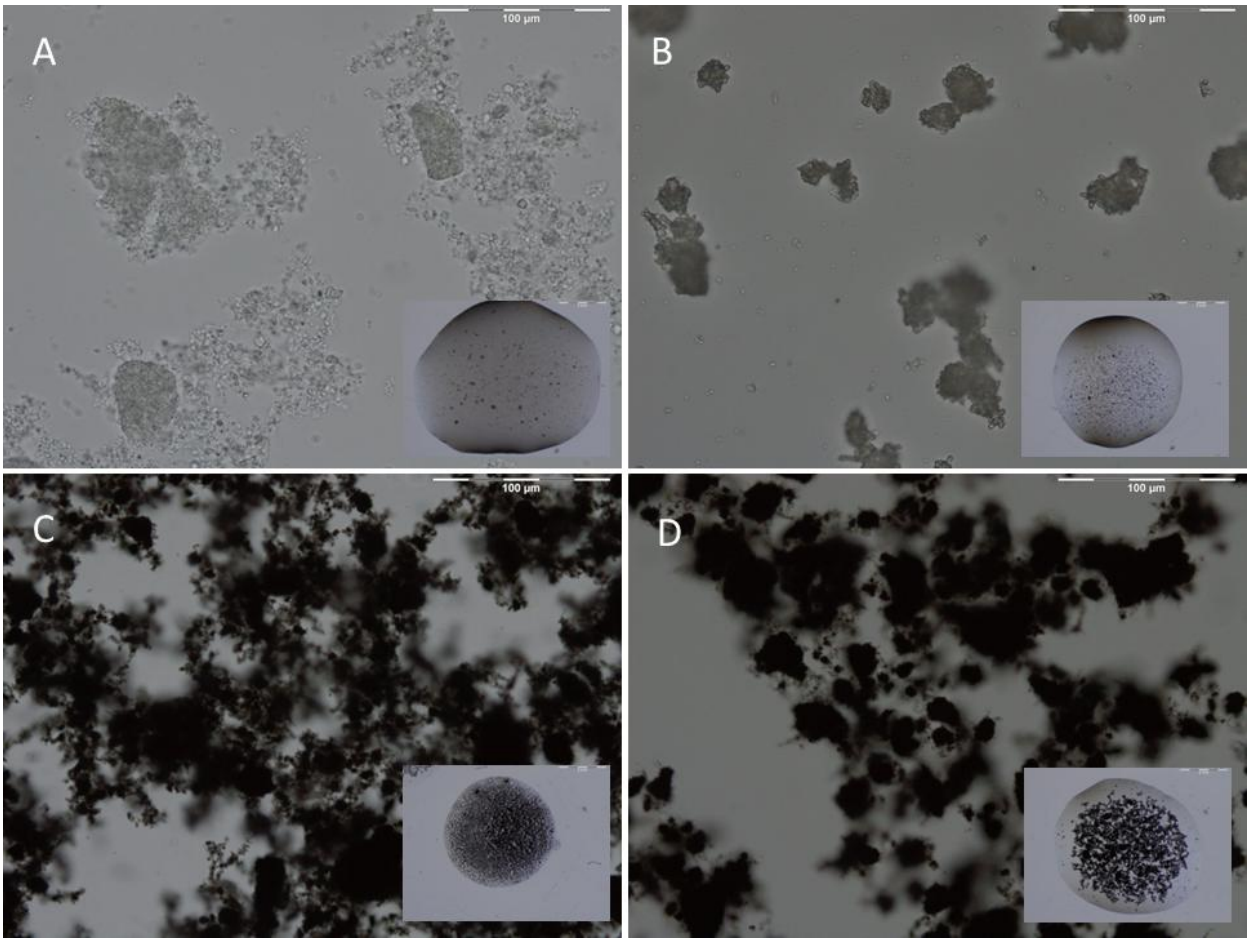

Figure 3. Nanoparticle dispersion in [C_4mmim][Tf_2N]. A) Al_2O_3 spheres, B) Al_2O_3 whiskers, C) carbon black, D) MWCNT

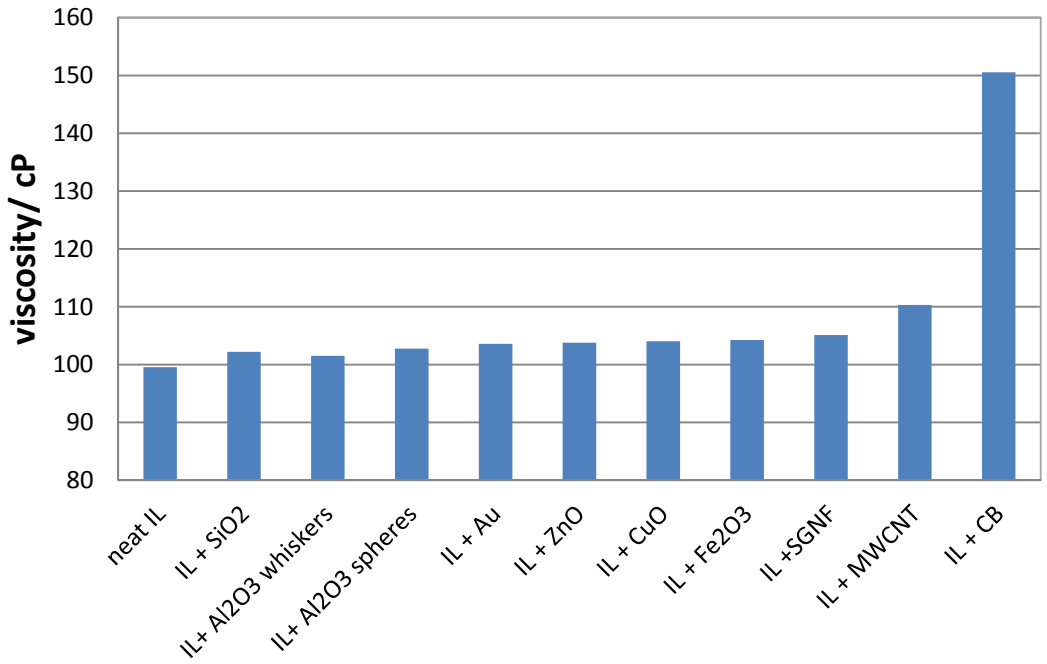

Figure 4. Viscosity of Neat IL and NEIL with 0.5 wt % nanoparticles

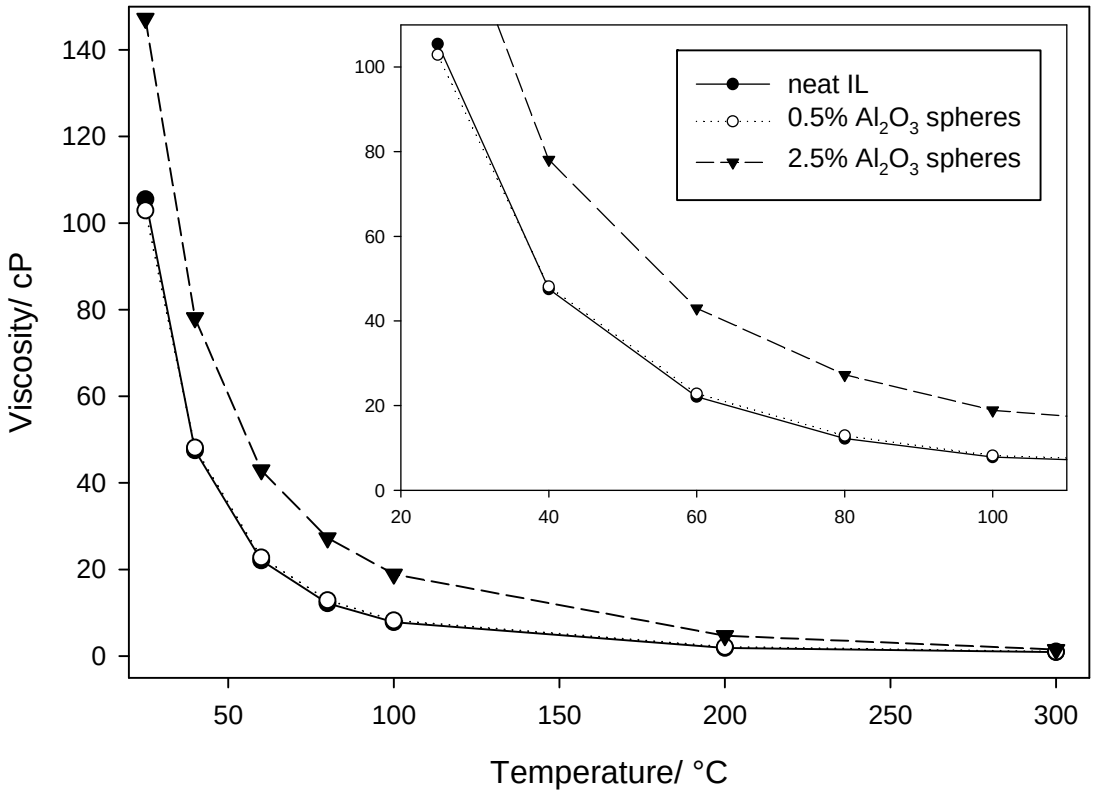

Figure 5. Effect of increasing concentration of Al_2O_3 spheres on $[C_4mmim][Tf_2N]$ viscosity versus temperature.

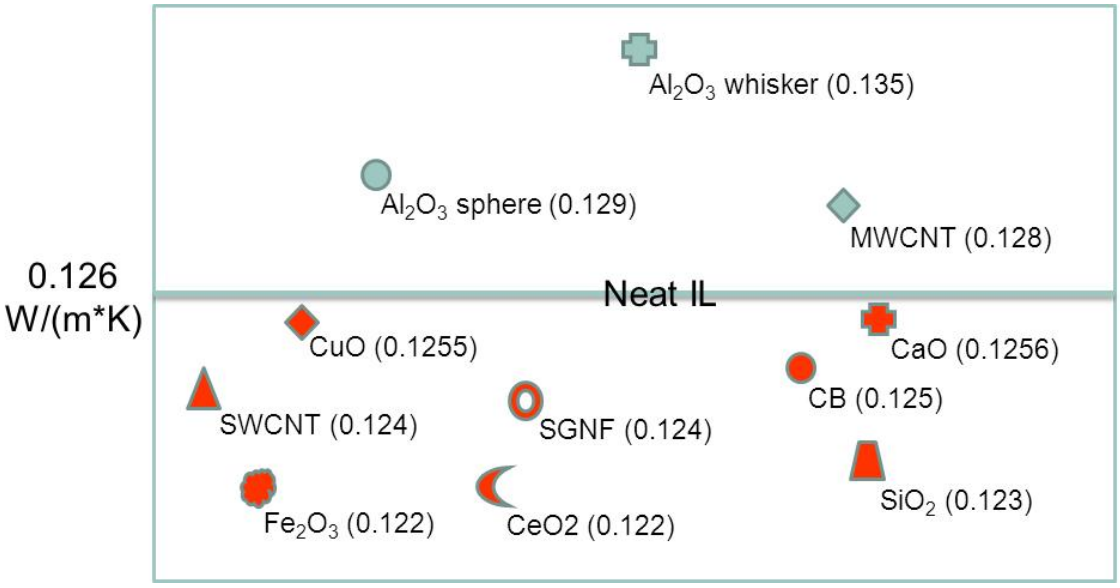

Figure 6. Thermal Conductivity (W/m*K) for NEILs Containing 0.5 wt % Nanoparticle at 50°C.

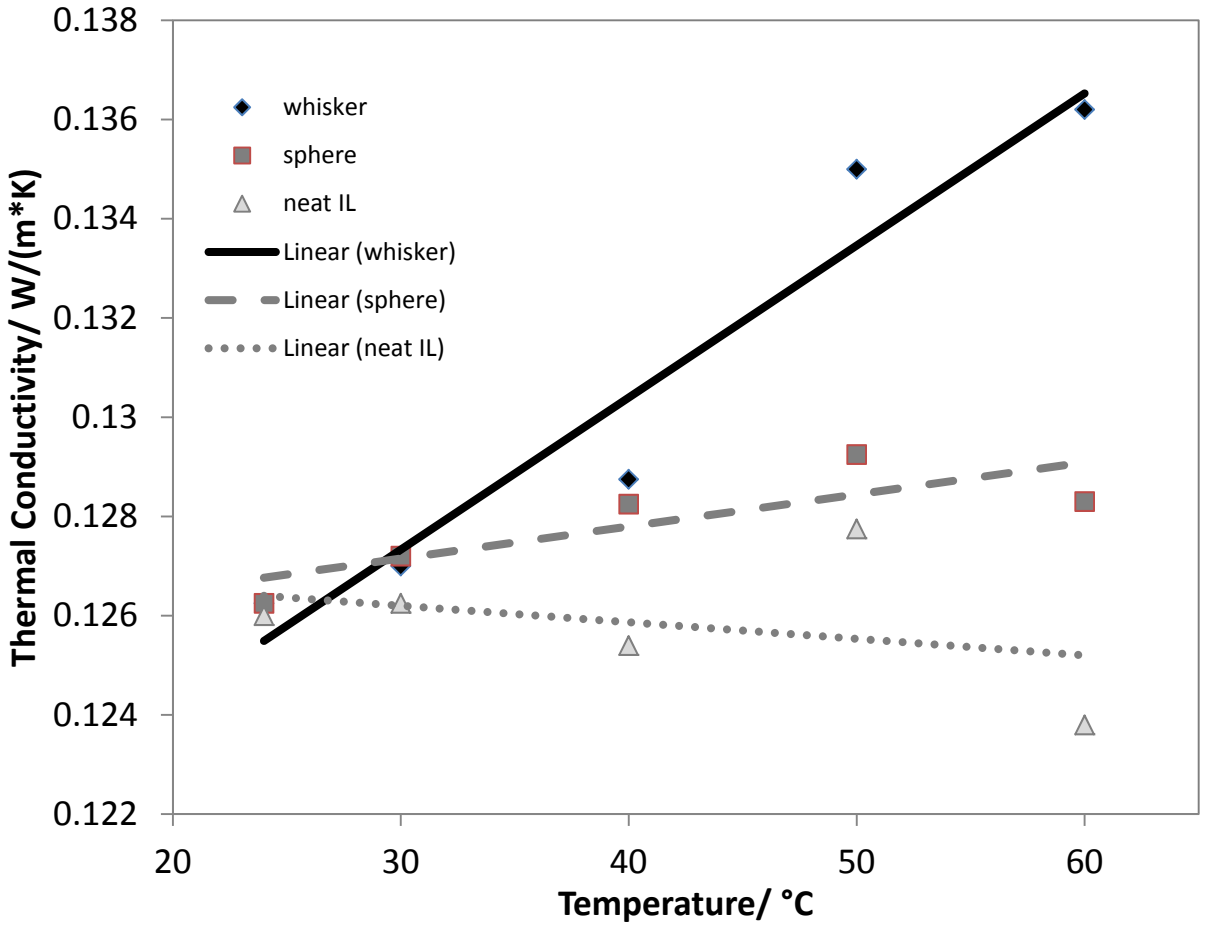

Figure 7. Thermal conductivity changes with increasing temperature for Al_2O_3 containing NEILs.

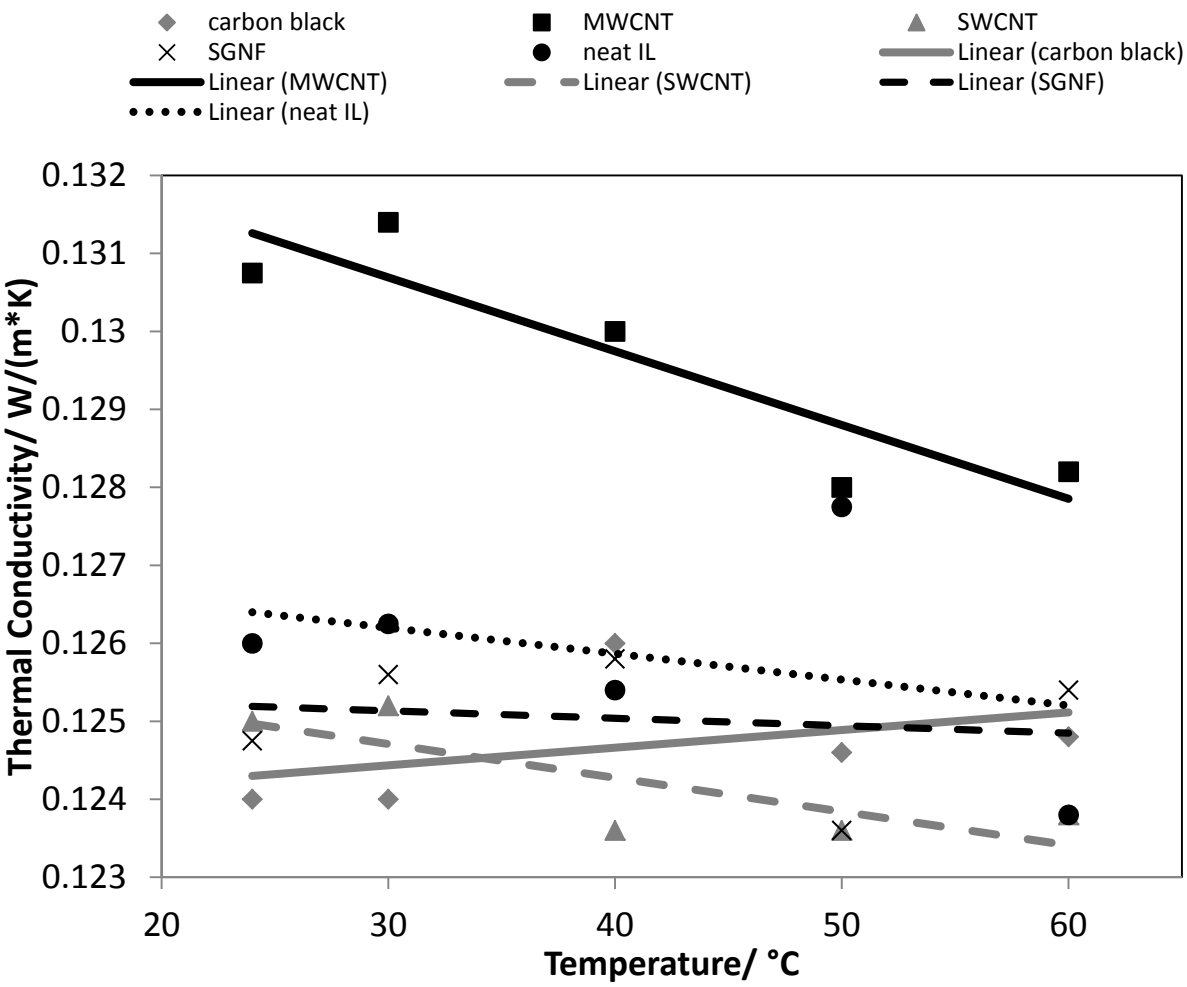

Figure 8. Thermal conductivity changes with increasing temperature for carbon containing NEILs.